Acta Biomaterialia 53 (2017) 598–609

Contents lists available at ScienceDirect

Acta Biomaterialia

journal homepage: www.elsevier.com/locate/actabiomat

Full length article

In vivo testing of gold nanoparticles using the *Caenorhabditis elegans* model organism

Laura Gonzalez-Moragas [a], Pascal Berto [b], Clara Vilches [b], Romain Quidant [b], Androniki Kolovou [c], Rachel Santarella-Mellwig [c], Yannick Schwab [c], Stephen Stürzenbaum [d], Anna Roig [a,*], Anna Laromaine [a,*]

[a] Institut de Ciència de Materials de Barcelona, ICMAB-CSIC, Campus UAB, 08193 Bellaterra, Barcelona, Spain
[b] ICFO-Institut de Ciències Fotòniques, Av. Carl Friedrich Gauss, 3, 08860 Castelldefels, Barcelona, Spain
[c] European Molecular Biology Laboratory, EMBL, Meyerhofstraße, 1, 69117 Heidelberg, Germany
[d] King's College London, Faculty of Life Sciences & Medicine, Analytical and Environmental Sciences Division, 150 Stamford Street, London SE1 9NH, United Kingdom

ARTICLE INFO

Article history:
Received 3 October 2016
Received in revised form 26 January 2017
Accepted 30 January 2017
Available online 1 February 2017

Keywords:
Biological interactions
Caenorhabditis elegans
Digestive system
Enterocytes
Endocytosis
Gold nanoparticles

ABSTRACT

Gold nanoparticles (AuNPs) are present in many man-made products and cosmetics and are also used by the food and medical industries. Tight regulations regarding the use of mammalian animals for product testing can hamper the study of the specific interactions between engineered nanoparticles and biological systems. Invertebrate models, such as the nematode *Caenorhabditis elegans* (*C. elegans*), can offer alternative approaches during the early phases of nanoparticle discovery.

Here, we thoroughly evaluated the biodistribution of 11-nm and 150-nm citrate-capped AuNPs in the model organism *C. elegans* at multiple scales, moving from micrometric to nanometric resolution and from the organismal to cellular level. We confirmed that the nanoparticles were not able to cross the intestinal and dermal barriers. We investigated the effect of AuNPs on the survival and reproductive performance of *C. elegans*, and correlated these effects with the uptake of AuNPs in terms of their number, surface area, and metal mass. In general, exposure to 11-nm AuNPs resulted in a higher toxicity than the larger 150-nm AuNPs. NP aggregation inside *C. elegans* was determined using absorbance microspectroscopy, which allowed the plasmonic properties of AuNPs to be correlated with their confinement inside the intestinal lumen, where anatomical traits, acidic pH and the presence of biomolecules play an essential role on NP aggregation. Finally, quantitative PCR of selected molecular markers indicated that exposure to AuNPs did not significantly affect endocytosis and intestinal barrier integrity.

Statement of Significance

This work highlights how the simple, yet information-rich, animal model *C. elegans* is ideally suited for preliminary screening of nanoparticles or chemicals mitigating most of the difficulties associated with mammalian animal models, namely the ethical issues, the high cost, and time constraints. This is of particular relevance to the cosmetic, food, and pharmaceutical industries, which all have to justify the use of animals, especially during the discovery, development and initial screening phases. This work provides a detailed and thorough analysis of 11-nm and 150-nm AuNPs at multiple levels of organization (the whole organism, organs, tissues, cells and molecules).

1. Introduction

Many of the products used in our daily life contain nanoparticles, gold nanoparticles (AuNPs) in facial creams [1], silver nanoparticles in preservatives [2], or zinc oxide nanoparticles and titanium dioxide nanoparticles in colorants and sunscreens [3]. For example, colloidal AuNPs hold great promise in cosmetics and as therapeutic and diagnostic agents due to their inertness (which limits their toxicity to cells) and their unique optical and photothermal properties. The latter can be controlled and tuned by changing the size, shape and surface functionalization of AuNPs [4,5].

AuNPs have been selected by the Working Party on Manufactured Nanomaterials of the Organization for Economic Cooperation and Development (OECD) as an example of

* Corresponding author.
E-mail address: alaromaine@icmab.es (A. Laromaine).

http://dx.doi.org/10.1016/j.actbio.2017.01.080
1742-7061/

manufactured nanomaterials which are either in commercialization or likely to enter the market in the near future [6]. Indeed, some AuNPs formulations have already been proposed as novel tools for *in vitro* and *in vivo* molecular imaging and drug delivery [7]. AuNPs have, for example, attracted interest as carriers to enhance the oral absorption of drugs and vaccines that are either poorly absorbed or are susceptible to gastrointestinal degradation [8]. However, to our knowledge, only AuNPs used for local heat generation in the plasmonic photothermal therapy of atherosclerosis and cancer have, to date, reached clinical stage (ClinicalTrials.gov Identifiers NCT01270139, NCT01679470, NCT00848042, NCT00436410) [9]. In addition, AuNPs are present in day to day products such as anti-ageing creams and masks, toothpastes, and are even marketed as food supplements according to the Consumer Products Inventory, which is compiled by the Project on Emerging Nanotechnologies [10]. However, the regulations on nanoparticles are being tightened and the use of animal-free alternatives to evaluate new materials is being actively promoted. For instance, in March 2013, EU regulations on Cosmetics and Household Products banned the use of animals to assess the safety of these products. The North American Food and Drug Administration (FDA) also supports the development and use of alternatives to animal testing to assess the safety of cosmetic products [11]. Hence, there is a pressing need to develop new platforms and approaches to evaluate AuNPs-containing products, in particular to hasten the early stages of safe nanoparticle development in the cosmetic, food, and pharmaceutical industries.

In this context, animal models such as *Caenorhabditis elegans*, *Drosophila melanogaster* or *Danio rerio* allow scientists to obtain primary data on engineered nanomaterials in a simple biological system, and in doing so they face less strict regulations and ethical issues compared to research conducted with mammals. These model organisms are compatible with high-throughput screens, even microfluidic technologies, which in turn accelerate the path of novel materials to the market [12,13]. *C. elegans* is a worm which exhibits 60–80% genome homology with humans and shares a multitude of biological traits in terms of physiology, anatomy, and metabolism (Fig. 1) [14,15]. The use of these 1-mm long animals, which naturally live in decaying organic matter in the soil, allows a cost-effective initial biological assessment of nanomaterials within chemical laboratories [16]. In addition, their transparency, small size, prolific and short life-cycle, and few requirements of maintenance facilitate the study of the interaction between nanomaterials and a multicellular organism [16]. The external part of the worm, the cuticle, can be used as a skin model given that its function and composition is analogous to human skin (Fig. 1A) [14,17,18]. The *C. elegans* intestine also shares a similar cellular architecture with higher animals with respect to cell polarity of the intestinal cells (enterocytes) including the presence of apical and basolateral domains, cell junctions, and the presence of microvilli forming the brush border (Fig. 1B). Setting aside some differences in the composition, both mammals and *C. elegans* encompass a pertrophic-like layer that protects the microvilar surface of the gut [14,19–23]. Furthermore, the mechanisms of transport of biomolecules through biological barriers are highly conserved [24–26]. Therefore, *C. elegans* offers promising features and valuable tools to evaluate the delivery of topical and oral nanomaterials before moving to more complex model organisms [16,27]. *C. elegans* can be used to track NPs through different biological barriers (dermal and intestinal) and multiple levels of organization (the whole organism, organs, tissues, cells and molecules).

Here, we report how advanced optical techniques such as two-photon luminescence microscopy (TPLM) [28], together with an array of materials science characterization techniques and state-of-the-art electron microscopy protocols [29] can be applied to study and quantify the nano/bio interaction between monodisperse small and large citrate-coated AuNPs in *C. elegans*. The biodistribution of AuNPs inside the worm was evaluated by microscopy at multiple scales, moving from micrometric to nanometric resolution and from organs to cells. These analyses were further complemented by investigating the effect of AuNPs on the survival and reproductive performance of *C. elegans*, which were correlated with the uptake of AuNPs. We determined NP status inside *C. elegans* using absorbance microspectroscopy and related the plasmonic properties of AuNPs with NP confinement in different anatomical areas within *C. elegans*. Finally, we selected several transcriptional markers to study whether AuNP exposure affects endocytosis and intestinal barrier integrity.

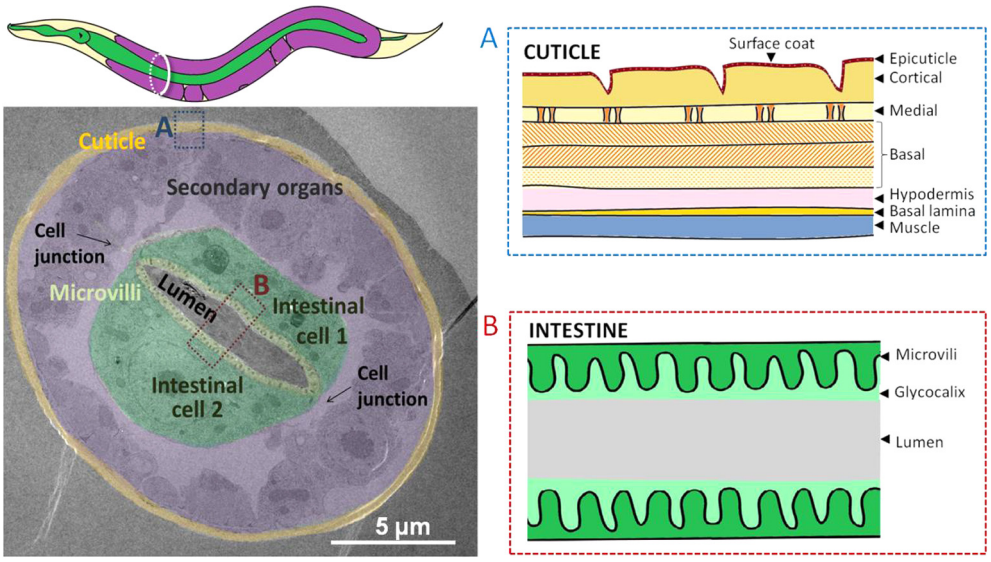

Fig. 1. Anatomy of *C. elegans*: the alimentary system, the cuticle, and secondary organs, including the reproductive system. Left panel shows a modified TEM image of a *C. elegans* cross-section, as marked in the drawing above. Right panel shows a magnification of A) the cuticle and B) the intestine, detailing their parts.

2. Methods

2.1. Materials

Caenorhabditis elegans Bristol strain N2 and *Escherichia coli* OP50 were obtained from the *Caenorhabditis* Genetic Center (CGC) stock collection, University of Minnesota, St. Paul, MN, USA. Peptone, yeast extract, bacteriological agar and tryptone were purchased from Conda Lab. All other reagents were bought from Sigma-Aldrich, if not stated otherwise.

2.2. Nanoparticle synthesis

The 11-nm citrate-coated AuNPs were synthesized by the Frens Turkevich synthesis, as described previously [30,31]. Briefly, 2 mL of an aqueous solution of trisodium citrate (Na_3C, 38.8 mM) were added to 20 mL of gold chloride ($HAuCl_4{\cdot}3H_2O$, 1 mM) at 100 °C under stirring. The solution was kept at 100 °C for 10 min or until it turned deep red. The 150-nm citrate-coated AuNPs were synthesized by seeded growth of 11-nm AuNPs. Two intermediate size steps were required (32 and 75 nm), as described previously [32].

2.3. NP characterization

2.3.1. Dynamic light scattering

Dynamic light scattering (DLS) and zeta potential measurements were performed with a Zetasizer Nano ZS (Malvern) with a He/Ne 633 nm laser at 25 °C. For each sample, Dynamic light scattering (DLS) and zeta potential measurements were performed with a Zetasizer Nano ZS (Malvern) with a He/Ne 633 nm laser at 25 °C. AuNP dispersions (100 μg/mL in MilliQ water) were sonicated for 5 min before the measurement. For each sample, three independent measurements were performed.

2.3.2. Transmission electron microscopy

AuNP dispersions (100 μg/mL in MilliQ water) were sonicated for 5 min, then 15 μL were placed on a copper grid. The copper grid was blotted with a filter paper and complete evaporation was allowed at room temperature. AuNPs were imaged with a JEOL JEM-1210 electron microscope at an operating voltage of 120 kV. About 200 different particles were computed to depict the size distribution and the mean size of AuNPs.

2.3.3. UV–Vis spectroscopy

A dispersion containing AuNPs in MilliQ water at 100 μg/mL was sonicated for 10 min in an ultrasound bath. Quartz cuvettes were employed in the measurements. UV–Vis spectra from 400 to 800 nm were acquired using a Varian Cary 5000 UV–Vis-NIR spectrophotometer. MilliQ water was used as blank to acquire the baseline spectra.

2.4. Exposure of C. elegans to AuNPs

2.4.1. Worm growth and exposure

Nematodes were grown on nematode growth medium (NGM) and fed *Escherichia coli* OP50 according to the standard protocol at 20 °C [33]. Each plate contained 1000–2000 animals. Synchronized young adult specimens (1-day adults) were treated with 100 μg Au/mL for 24 h in MilliQ water in 24-well plates, per triplicate, in a final volume of 0.5 mL/well.

2.4.2. AuNPs uptake

~2000 exposed worms were thoroughly washed 4 times with fresh MilliQ water, then pelleted in a polycarbonate capsule by centrifugation (1 min at 1300 rcf) and dried overnight at 60 °C. The sample was digested with 0.5 mL aqua regia at 150 °C, and digestions blanks were performed in parallel. Finally, the volume was adjusted to 10 mL. The gold content of the resulting solution was determined in duplicate using inductively coupled mass plasma spectrometry (ICP-MS) with an Agilent 7500ce spectrometer. Final concentration of HCl was of 1% in all the samples and standards analyzed. The operational conditions and standards used are indicated in Table S1.

2.4.3. Zeta potential measurements

~25 synchronized young adult *C. elegans* were introduced in a Zeta potential cuvette filled with MilliQ water by picking them individually from NGM plates under the stereoscope. The measurements were performed with a Zetasizer Nano ZS (Malvern) with a He/Ne 633 nm laser at 25 °C. For each sample, three independent measurements were performed.

2.4.4. Scanning electron microscopy–energy-dispersive X-ray spectroscopy analysis

Treated worms were fixed with 4% paraformaldehyde in MilliQ water for 2 h at room temperature, then washed three times with MilliQ water, and concentrated to 100 μL by centrifugation (1 min at 1300 rcf). A sample (20 μL) was transferred to a piece of carbon tape placed on an aluminium stub, and dried at room temperature. SEM-EDX analyses were carried out with a scanning electron microscope (QUANTA FEI 200 FEG-ESEM) equipped with an energy-dispersive X-ray (EDX) system. SEM was used under low vacuum conditions, an acceleration voltage of 10 kV, and an electron beam spot of 3.0.

2.4.5. Biodistribution assay

Treated worms were fixed with 4% paraformaldehyde in MilliQ water for 2 h at room temperature, then washed three times with MilliQ water, mounted on a glass slide with aqueous mounting media (Fluoromount®) and observed under the microscope. A Zeiss Axio Observer Optical Microscope in transmission mode was used to detect visible accumulation of AuNPs inside treated *C. elegans*.

2.4.6. Two-photon luminescence microscopy

A TPLM based on a commercial Leica TCS SP5 confocal system, coupled to a MIRA 900F Ti:Sa laser source (Coherent), was used to acquire the two-photon luminescence of AuNPs inside *C. elegans*. The femtosecond laser beam was tuned in the near infrared (λ = 800 nm) and focused onto the sample by means of a microscope objective (HCX PL APO 10x/0.40 CS). The epi-collected luminescence signal was acquired in the 400–700 nm range with a hybrid detector (HyDs, Leica). Each image was taken in a 1024 × 1024 pixel format and a scanning speed of 200 Hz. Z-stacks were collected in 6.5 μm step size and processed using Image J software. Average power in the sample plane was measured to be 12 mW. Under these experimental conditions, endogeneous two-photons autofluorescence of the worms was weak and negligible compared to the strong two-photon luminescence of AuNPs (Video S3).

2.4.7. Absorbance microspectroscopy

C. elegans were mounted as described above, visualized using an Olympus BX51 microscope and spatially resolved absorbance spectroscopy was performed by fiber-coupling the signal to a spectrometer (Shamrock SR-303i-B with Andor Solis camera: iDus DV401A-BV). The sample, illuminated in bright field geometry, was imaged at the entrance of the optical fiber to reduce the collection area to a 10-μm spot size. Spectra were background subtracted against and normalized with a reference spectrum (the glass slide). The spectra of ten worms per condition were acquired using 1000 s accumulation per triplicate.

2.4.8. Toxicological assays

We assessed survival (lethal endpoint) and brood size (sub-lethal endpoint). In the survival assay, animals were treated with 100 μL MilliQ water (controls) or 100 μg Au/mL in MilliQ water (treated worms) in 96-well plates for 24 h. The assay was performed in triplicate. The plates were tapped and the worms that moved were counted as alive. Each well contained 9 ± 3 young adult worms. To study brood size, individual untreated or treated young adult worms were transferred to a NGM plate seeded with an OP50 lawn at 20 °C. The number of progeny was scored after 72 h of food resumption. Results are expressed as percentage brood size in respect to the untreated (control) worms. The reprotoxicity assay was performed in triplicate.

2.4.9. Excretion of AuNPs

After treatment for 24 h, 6–7 worms were transferred to an NGM plate with *E. coli* OP50. Excretion of the internalized AuNPs was monitored under the light microscope up to 12 h after food resumption, based on the visible pink and blue color of the 11-nm AuNPs and 150-nm AuNPs, respectively.

2.4.10. Correlative light electron microscopy (CLEM)

The cellular localization of AuNPs in *C. elegans* was investigated by correlated light and electron microscopy (CLEM). Control and treated animals were fixed by high-pressure freezing, flat-embedded in resin, and sectioned following a targeted ultramicrotomy protocol, as described previously [29]. Imaging was performed with a PHILIPs CM 120 transmission electron microscope.

2.4.11. High angle annular dark field scanning transmission electron microscopy (HAADF STEM)

The prepared cross-sections of *C. elegans* were also visualized by means of HAADF STEM using the Magellan XHR SEM 400L at 20 kV in STEM mode, at a working distance of 4.2 mm and a current of 0.10 nA.

2.4.12. Quantitative PCR (qPCR)

Total RNA was extracted using Tri-reagent (Sigma-Aldrich) from worms exposed to 100 μg/mL 11-nm AuNPs for 24 h in 50% M9 buffer (treated worms) or without NPs (control worms). cDNA was synthesized and quantitative PCR of *elt-2, eps-8, act-5, chc-1* and *dyn-1* was performed using an ABI Prism 7500 FAST platform (Applied BioSystems). All probes were sourced from the Universal ProbeLibrary (Roche) and primers were designed using the Assay Design from Roche (Table S2). We applied the $\Delta\Delta C_T$ method to calculate the fold change in gene expression for each gene. The gene *rla-1* was used as reference gene. Three biological replicates were analyzed, and four technical repeats were used per sample. Further details of the qPCR methods can be found in the Supplementary data.

2.5. Statistical analysis

Past 3.03 was used for all statistical analyses. For the toxicological assays, statistical significance between control and treated worms was assessed using the Student's *t*-test. Three levels of statistical significance were considered in all cases: $p < 0.05$ (∗), $p < 0.01$ (∗∗), and $p < 0.001$ (∗∗∗).

3. Results and discussion

3.1. Characterization of the material

The 11-nm citrate-coated AuNPs were synthesized by the Frens Turkevich reaction, as described previously [30,31]. The 150-nm citrate-coated AuNPs were obtained by seeded growth (Fig. S1) [32]. Citrate coating is also used in some commercial colloidal gold formulations [34,35]. The two AuNPs systems were well characterized; obtaining a nominal size for the AuNPs of 11 ± 1 and 150 ± 17 nm (by TEM); a hydrodynamic mean diameter of 16 ± 3 and 221 ± 49 nm (by DLS); a zeta potential of −26.4 and −21.2 mV; and a maximum resonance plasmonic absorption band at 525 and 598 nm (by UV–Vis), respectively (Fig. 2).

3.2. C. elegans exposure to AuNPs

C. elegans were fed with AuNPs in aqueous dispersion for 24 h. During feeding, *C. elegans* pumps liquids by rhythmic contractions of the pharynx to the lumen of the intestine [14]. AuNPs were introduced gradually through the alimentary system and accumulated over a period of 24 h. Toxicological effects were evaluated by means of survival and brood size assays. We quantified the ingestion of gold by inductively coupled plasma mass spectrometry (ICP-MS) and investigated the interaction between the external surface of *C. elegans*, the cuticle, and the AuNPs using scanning electron microscopy (SEM), energy-dispersive X-ray (EDX) spectroscopy, and zeta potential measurements. The pharyngeal cuticle was studied by TEM, and the biodistribution of AuNPs evaluated by light microscopy (LM), TPLM, and TEM, from lower to higher spatial resolution. Remarkably, TEM investigations allowed us to track NP fate at the cellular and subcellular levels, and to evaluate the crossing of biological barriers with single-NP resolution. Finally, the optical status of AuNPs was determined by absorbance microspectroscopy on individual worms utilizing a custom-designed setup as described in the Methods section.

3.3. Toxicity and uptake

The biocompatibility of the material was evaluated by studying two toxicity endpoints, survival and reproductive performance (brood size), in young adults. We assessed AuNPs in the concentration range 0–500 μg/mL and observed that 100 μg/mL induced a significant decrease in the survival of 11-nm AuNPs treated worms, compared to control animals (Fig. S2), hence we selected this concentration to evaluate the effect of AuNPs in *C. elegans*. A treatment of 100 μg/mL of the small nanoparticles also significantly decreased the reproductive output. Survival and brood size decreases were not statistically significant in the case of the larger AuNPs (Fig. 3A). In a previous work, we found that citrate, at the concentration used here, does not affect *C. elegans* [36] while Na^+ concentration was kept constant between all the conditions (control, 11-nm and 150-nm AuNPs). In addition, it is well accepted that the dissolution of AuNPs is negligible in acidic biological systems [37,38]. Hence, we attribute the effects on survival and brood size solely to the AuNP treatment. Previous studies on Ag-NPs also reported toxicity for *C. elegans* survival and reproduction at similar metal doses [39], while other compositions such as iron oxide were more biocompatible (up to five fold in terms of metal weight) [36,40]. Similarly, other authors reported that smaller NPs (⩽10 nm) were more toxic to *C. elegans* than larger NPs (⩾50 nm) [41,42].

We quantified the uptake of NPs by chemical analysis and found that worms ingested 500 times more 11-nm AuNPs than 150-nm AuNPs. However, the gold mass contained in the worm's body was nearly seven times higher in the case of the large NPs due to the size of the ingested particles. Given that the surface area of ingested NPs was twice as high in worms treated with the 11-nm AuNPs compared to worms exposed to 150-nm AuNPs, and the fact that gold surface atoms are highly reactive, might account for the observed nanotoxicity of the smaller NPs (Fig. 3B and Table S3). Moreover, studies on other inorganic NPs suggested that

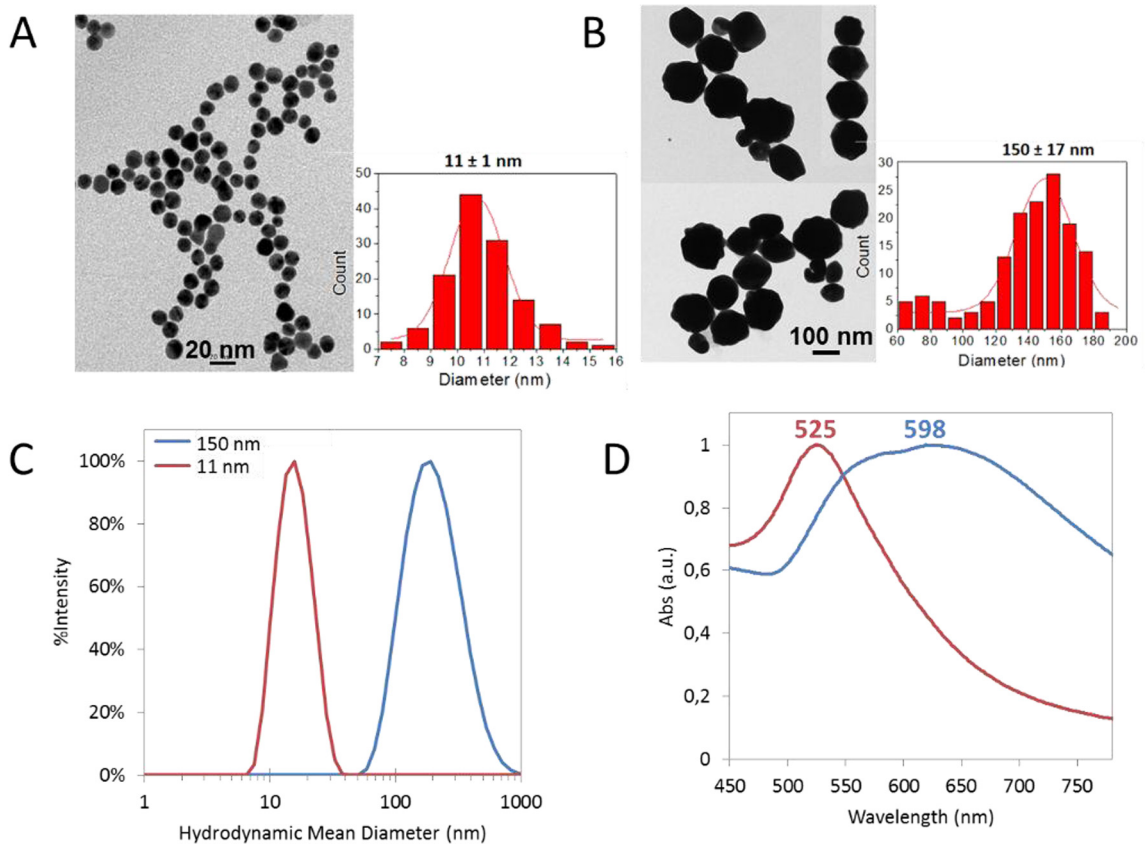

Fig. 2. Characterization of the small and large AuNPs. A) TEM image and size distribution of 11-nm AuNPs. B) TEM images and size distribution of 150-nm AuNPs. C) DLS measurements. D) UV–Vis spectra.

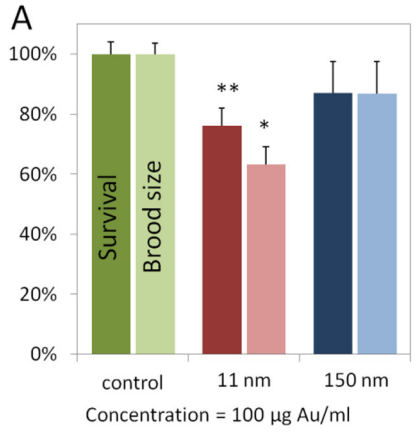

B AuNP uptake (per worm)

	11-nm AuNPs	150-nm AuNPs	ratio 11/150
Metal amount (pg Au)	738 ± 78	4850 ± 248	0.15
Number of NPs (x 10^6)	70 ± 7	0.14 + 0.01	500
Surface area of ingested NPs (x 10^{10} nm^2)	2.3 ± 0.2	1.0 ± 0.1	2

Fig. 3. A) Survival (bold colors) and brood size (pale colors) of *C. elegans* grown in the presence or absence of 11-nm and 150-nm AuNPs (100 µg/mL). Significant differences are only observed in worms exposed to the 11-nm AuNPs. Error bars indicate standard error of the mean (SEM) (n = 3). $^{*}p < 0.05$, $^{**}p < 0.01$, $^{***}p < 0.001$. B) AuNPs uptake by chemical analysis. Results are presented as picograms of Au, number of NPs and surface area of ingested NPs per worm. Error bars indicate standard deviation (SD) (n = 3). (For interpretation of the references to colour in this figure legend, the reader is referred to the web version of this article.)

smaller particles (up to 10 nm) can trigger oxidative stress to a greater extent than larger particles, mainly due to their larger surface area [41,42].

In terms of NP uptake per body mass, *C. elegans* ingested 6–42 × 10^5 µg/kg AuNPs, corresponding to a metal dose which is 5–6 orders of magnitude above the maximum prescribed dose for humans. For instance, MesoGold®, marketed in the US as a mineral supplement to enhance the body's immune system, contains a dispersion of 3.2-nm AuNPs at 20 µg/mL (250 mL), with the recommended adult daily dosage being 4–17 µg/kg. The worms were treated with metal doses exceeding the human doses, suggesting that the AuNPs are biocompatible. Furthermore, this study emphasises that *C. elegans* can serve as a surrogate animal model, since vertebrates could not be treated under these harsh conditions due to ethical concerns; *C. elegans* can thus fill a gap within toxicological evaluations, despite being a simple organism.

3.4. Interaction with the external and pharyngeal cuticle

The interaction between the external surface area of *C. elegans* and AuNPs was investigated by SEM-EDX (Fig. 4). The outer surface of *C. elegans* is covered by an extracellular cuticle, which separates

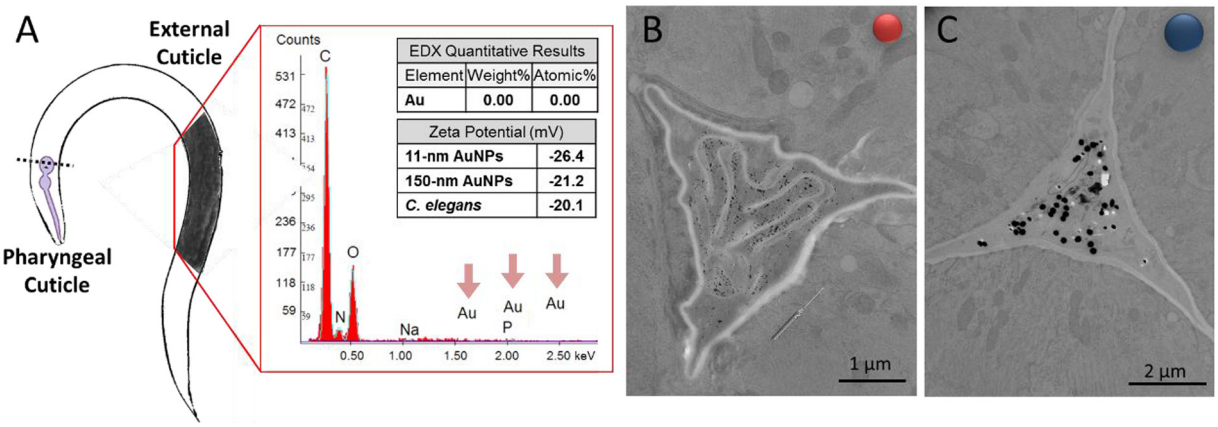

Fig. 4. A) Representative SEM-EDX analysis of the interaction between the external cuticle and AuNPs. After extensive washing of the worms with MQ water, no traces of gold is detected on the outer surface of *C. elegans*. B, C) TEM images showing the interaction between the pharyngeal cuticle and 11-nm (red sphere, panel B) or 150-nm AuNPs (blue sphere, panel C). (For interpretation of the references to colour in this figure legend, the reader is referred to the web version of this article.)

the interior of the body from the environment and acts as an external skeleton [14]. The epidermis of invertebrates is the primitive predecessor of skin in humans and all other vertebrate animals, both structurally and functionally. Therefore, the cuticle and epithelia of *C. elegans* have been used as a simplified skin model for NP assessment *in vivo* [17,18]. The cuticle comprises five layers, mostly consisting of collagen, lipids, and some glycoproteins (Fig. 1A). Structural proteins and lipids are also present in human skin, whereas other components (i.e. keratin or elastin) are specific to mammals [14]. The cuticle possesses a negative surface charge, confirmed by a zeta potential of –20.1 mV for *C. elegans* in MilliQ water. EDX quantitative analysis revealed that AuNPs did not attach to the external surface of the animal (based on the absence of gold). The negative charge of both the cuticle and the citrate-capped AuNPs may explain the lack of affinity between them [14]. Hence, these results imply that NPs do not enter via the dermal route and indicate that the alimentary tract is the main portal of NP entry into the body of the worm in our experiments. The *C. elegans* cuticle also covers the four major openings of the body to the exterior: the anus, the excretory pore, the vulva and the pharynx. However, unlike previous studies using fluorescent SiO_2-NPs [43,44], we did not observe entrance of NPs through other body openings. The interaction between the pharyngeal cuticle and the AuNPs was investigated by TEM. Adhesion of AuNPs to the pharynx was unlikely, as NPs were distributed inside the pharyngeal lumen and did not attach to the cuticle (Fig. 4B, C).

3.5. Biodistribution

AuNPs were introduced gradually to the alimentary system and accumulated for up to 24 h in the intestinal lumen. When visualizing AuNPs inside the intestinal lumen of *C. elegans* under transmitted light from a light microscope (LM), the colors of the 11-nm AuNPs appeared pink and the 150-nm AuNPs blue, which is consistent with their absorbance in the UV–Vis (Figs. 5B–C and S3). Although the intensity of the color was not uniform throughout the body, no appreciable color change occurred inside *C. elegans*. However, both 11 and 150-nm AuNPs appeared redder in reflected light, likely due to scattering effects. Absorbance microspectroscopy was employed to obtain a more precise analysis of the optical properties of AuNPs inside the worm.

Exploiting the luminescent properties of AuNPs, we performed TPLM studies to analyze the NP uptake in individual worms at different segments of the intestinal tract, namely the pharynx, the anterior gut, the mid-gut, the posterior gut, and the rectum (Fig. 5A). Each segment of the intestinal tract is characterized by a different pH value [45]. Under near-infrared pulsed illumination, AuNPs luminesce via interband transitions induced by the absorption of two photons. This signal is strongly enhanced when the pulsed illumination spectrally overlap with the localized plasmon resonance of the AuNPs [46–50]. TPLM is of particular interest as it can provide improved AuNPs contrast compared to bright-field or dark-field microscopy, which are often hampered by the endogeneous parasitic scattering of the worms. Furthermore, as multiphoton processes feature a nonlinear dependence on the excitation intensity, TPLM is intrinsically confocal and offers three-dimensional imaging capabilities with improved spatial resolution.

TPLM allows us to visualize AuNPs in a cellular environment [51], with single-particle sensitivity [52]. This method has been widely used to image functionalized AuNPs targeting cancer cells *in vitro* [50,53] and AuNPs distribution in mice *in vivo*,[52,54] but rarely to localize AuNPs inside *C. elegans* [28]. Here, TPLM images indicated the confinement of AuNPs in the intestine of *C. elegans* and the absence of AuNPs outside the intestinal lumen. By scanning the sectioning plane of the TPLM image, TPLM tomography allowed a three-dimensional reconstruction of the entire worm, confirming the absence of AuNPs adsorbed onto the cuticle and excluding a topical entrance of AuNPs (Fig. 5D, E, and Videos S1, S2, S3). Therefore, the toxicological effects of AuNPs can only be attributed to the AuNPs present in the digestive tract of *C. elegans*, and their status (aggregation, surface area, etc.) may play a determining role.

3.6. NP localization at the cellular scale

Ultrathin cross-sections of treated worms were examined by TEM to study the subcellular localization and size of AuNPs inside *C. elegans* and, in doing so, to determine whether AuNPs are capable of crossing the intestinal barrier. In all cases, AuNPs preserved their monodispersity, were restricted to the intestinal lumen and not internalized by the intestinal cells (Fig. 6B–E). We did not visualize NP-containing endosomes, and the particles remained separate from the microvilli by a peritrophic-like membrane, the glycocalix, which protects the intestinal cells against foreign materials, mechanical injury, and pathogens. This extracellular electronlucent coating consists of highly modified glycoproteins, which localizes digestive enzymes and filters the molecules that reach the absorptive surface of the microvilli [23,55]. Borgonie et al. investigated the passage of different molecules through this

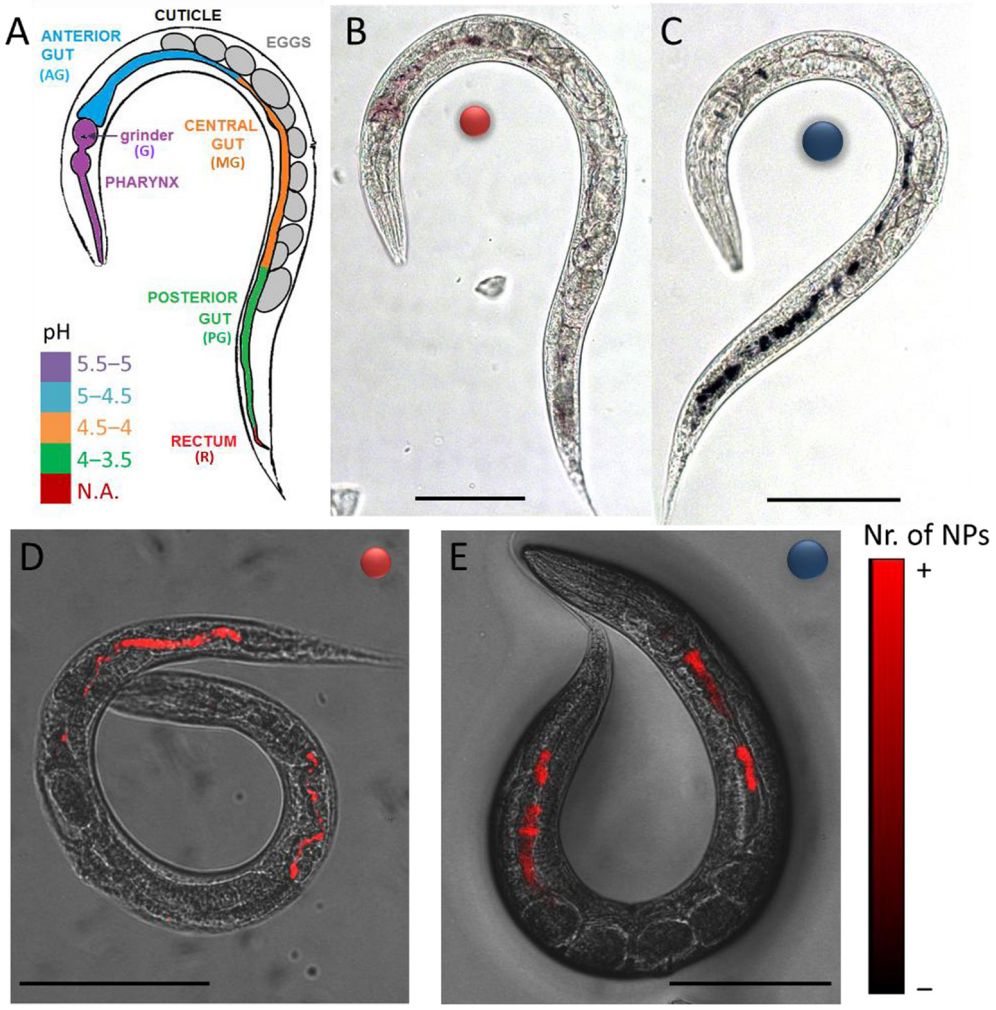

Fig. 5. A schematic drawing of the anatomical parts under evaluation (panel A). The intestinal tract is segmented into five parts, depicted with various colors according to their pH: pharynx, which contains the grinder; the anterior, mid and posterior parts of the gut, and the rectum. Panels B and C are optical microscopy images of B) 11-nm and C) 150-nm AuNPs treated worms. 11-nm AuNPs appear pink, and 150-nm AuNPs appear blue. Panels D and E are TPLM images of D) 11-nm and E) 150-nm AuNPs treated worms, areas with higher accumulation of nanoparticles are seen in red confirming the absence of AuNPs adsorbed onto the cuticle and excluding topical entrance of AuNPs. Scale bars correspond to 100 μm. (For interpretation of the references to colour in this figure legend, the reader is referred to the web version of this article.)

protective layer and observed only sparse crossing of ferritin molecules, while it allowed passage of fluorescein isothiocyanate, methyl red, neutral red, and acridine orange [22]. High-angle annular dark-field scanning transmission electron microscopy (HAADF STEM) of animal cross-sections confirmed the absence of NP endocytosis and translocation, as AuNPs were only visualized in the intestinal lumen (Fig. S4).

Endocytosis or translocation to secondary organs in *C. elegans* have been reported for oxide nanoparticles such as citrate-capped 6-nm Fe_2O_3-NPs [36,56] 50-nm SiO_2-NPs [44], and carbon nanomaterials including graphene oxide [57], bioconjugated nanodiamonds [58], or carbon nanotubes.[59] Also, endocytic trafficking of metal NPs such as citrate-capped 7-nm Ag-NPs [60] or 4-nm AuNPs [61] has been documented. We tracked AuNPs of two different sizes by a range of techniques and in all cases concluded that no endocytosis occurred within the 24 h incubation period. The absence of internalization of NPs by the intestinal cells of *C. elegans* could be attributed to the lower transcytotic capacity of the *C. elegans* intestine compared to that of vertebrates. Recent studies in mammals have revealed that the Microfold cells (or M cells) present in the intestinal barrier, which lack the glycocalyx covering and have a poorly organized brush border, are necessary for the absorption of NPs that are administered orally (Fig. S5) [62]. While little translocation occurs through the enterocytes, especially for negatively charged particles, the coexistence of enterocytes and M cells can increase NP absorption by up to 50-fold [8,63]. The absence of M cells in *C. elegans* could explain the deficiency of AuNPs translocation. To support the lack of endocytosis of AuNPs, we assessed molecular markers of endocytosis (*chc-1, dyn-1*, *eps-8*) and intestinal barrier integrity (*eps-8, act-5, elt-2*) by qPCR (Fig. 7), genes previously reported to be affected by 4-nm citrate-coated AuNP treatment in *C. elegans* [61]. To validate the qPCR integrity of total RNA/cDNA, positive controls included metal-responsive transcripts (*mtl-1, mtl-2, ftn-1, ftn-2*). We found no significant alteration in the gene expression patterns of the above mentioned endocytosis and intestine markers between control and treated worms, except for *act-5* (actin). The expression of *act-5* is limited to intestinal tissue and is essential for microvilli formation. It is conceivable that the down-regulation of *act-5* may be induced by the presence of AuNPs in the intestine, in proximity to the microvilli. In contrast, the expression of *elt-2*, the dominant transcription factor controlling differentiation and function of the *C. elegans* intestine, was not significantly affected by NP treatment [64,65]. The lack of endocytosis observed by TEM is supported by the basal expression of *dyn-1* (dynamin), involved in the early stages of endocytosis; *chc-1* (chlatrin), involved in vesicle formation during

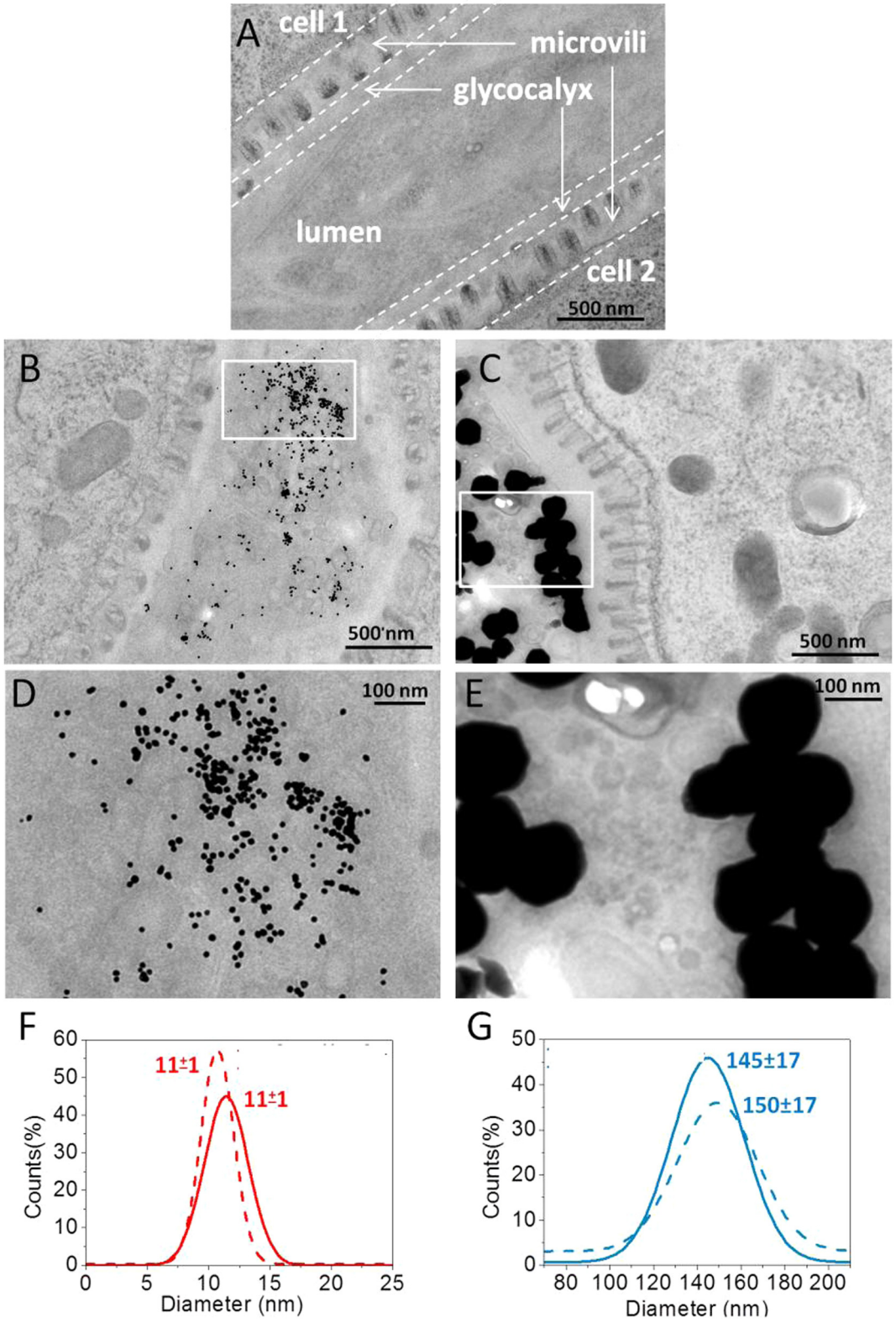

Fig. 6. TEM section of the anterior part of the intestine of A) control nematodes, B) nematodes treated with 11-nm and C) 150-nm AuNPs. Images at higher magnification of D) 11-nm AuNPs and E) 150-nm AuNPs. TEM size distributions of F) 11-nm AuNPs as synthesized (dotted lines) and inside *C. elegans* (solid lines) and G) 150-nm AuNPs.

endocytic transit; and *eps-8*, located at the microvilli tips and associated with endocytosis. However, our findings are different from those reported by Tsyusko et al., who identified an endocytic pathway in the response of *C. elegans* to 4-nm citrate AuNPs. Although we both used 50% M9 buffer as exposure media, there are several methodological differences that may account for the different experimental outcomes. Firstly, they used 4-nm AuNPs, while our 11-nm AuNPs are almost three times larger in diameter and >20 times larger in volume. Moreover, they exposed the worms to lower concentrations of AuNPs, corresponding to LC_{10}, for 12 h and allowed treated animals to recover for 12 h. In our case, we incubated worms to a higher concentration, close to LC_{30}, for a

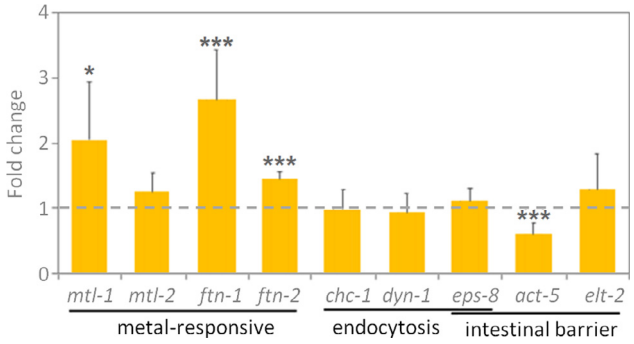

Fig. 7. Gene expression fold change of metal-responsive genes (*mtl-1, mtl-2, ftn-1, ftn-2*), endocytosis genes (*chc-1, dyn-1, eps-8*) and intestinal barrier integrity genes (*eps-8, act-5, elt-2*) in worms exposed to 11-nm AuNPs, evaluated by qPCR. Three biological replicates were analyzed, and four technical repeats were used per sample. Error bars indicate the standard error of the mean (SEM). Dotted line at 1 indicates the normalized base-line expression level of control animals. T tests were used to compare treated and untreated worms and determine the p value. $^{*}p < 0.05$, $^{***}p < 0.001$.

longer period (24 h) without recovery. We exclude AuNP endocytosis based on the fact that we did not observe the triggering of this pathway in *C. elegans* either by means of electron microscopy or qPCR. Studies in superior animal models reported scarce or no translocation of gold nanoparticles after oral administration depending on the dosing regime, NP size and surface properties but without a clear trend [66,67]. Therefore, we believe NP size can also have an influence in *C. elegans*, together with the exposure concentration and the presence/absence of recovery time.

Based on the TEM images, no size decrease of the NP core was observed, which confirms that AuNPs are neither degraded nor digested in the intestinal microenvironment of *C. elegans*, at least within 24 h (Fig. 6F, G). Other NPs such as iron oxide NPs or quantum dots are metabolized inside the *C. elegans* intestine and suffer size decrease or structural collapse [36,68]. The unchanged size of the AuNPs also indicates that both sizes of NPs pass through the pharyngeal grinder, suggesting that it is only able to break up biological entities such as bacteria but not inorganic materials, which supports previous results obtained with 3-μm latex beads [69].

The monodispersity of the AuNPs inside *C. elegans* and the absence of necking between them suggest that the citrate coating was preserved inside the worm, which hence indicates a strong electrostatic interaction between the metallic core of the NP and the surfactant. *In vitro* evaluation of AuNPs in simulated *C. elegans* intestinal conditions confirmed those results. We mimicked the intestinal *C. elegans* microenvironment by incubating the 11-nm AuNPs for 24 h at pH 4.6 with and without 10% fetal bovine serum (FBS). DLS measurements demonstrated that 11-nm AuNPs aggregated under the simulated conditions ranging from an initial hydrodynamic mean size of 10 ± 2 nm in MilliQ water to 900 ± 300 nm in citrate buffer at pH 4.6. In contrast, aggregation was reduced (180 ± 60 nm) when FBS was incorporated into the system. UV–Vis spectroscopy revealed a 59-nm red-shift of the maximum absorbance peak when AuNPs were incubated without protein and a mere 6-nm peak shift when FBS was added. TEM analysis further confirmed the degree of aggregation (Fig. S6). This *in vitro* study supported our hypothesis that the pH of the specific region of the intestine and the biomolecules present (i.e., proteins) enhance the stability of the AuNPs and prevent the formation of large aggregates, as observed *in vivo* in the *C. elegans* intestine.

3.7. NP status inside C. elegans

AuNPs have a strong tendency to form large aggregates, especially when they are exposed to highly ionic media. We wanted to evaluate the behaviour of citrate-capped AuNPs *in vivo* in a multicellular biological environment (taking into account ionic strength, pH, space constriction, etc.) and to determine the resulting effects on the material. NP aggregation inside *C. elegans* was monitored by absorbance microspectroscopy measurements along the body of treated worms, in particular at the grinder, the anterior, central and posterior parts of the gut, and the rectum. Aggregation induces a coupling of the AuNPs' plasmon resonance modes, which results in a red shift and broadening of the plasmon resonance [70]. By using a home-made setup consisting of a UV–Vis spectrometer coupled to an optical microscope, we were able to acquire spectra of the AuNPs in the targeted areas of individual *C. elegans* with 10-μm precision. At least ten worms per condition were analyzed and the mean spectrum for each part of the worm was plotted (Fig. 8A).

Plasmon resonance peak shifts were used to evaluate the aggregation level of the AuNPs when confined in the different anatomical regions. Interparticle distance changed according to the physioanatomical properties and pH of the different areas of the intestinal tract, inducing specific degrees of aggregation in each region (Fig. 8B and Table S4). In all cases we observed a broadening of the absorption band and a red-shift of the peak maxima. No AuNPs were detected by spectroscopy in the reproductive organs.

In the grinder, the 150-nm AuNPs displayed the highest peak shift, due to the space constriction of the pharyngeal lumen. The grinder is made up of three pairs of muscle cells that rotate when the muscles contract and act as "teeth" that break up food [14]. When closed, the pharyngeal lumen is constrained to a diameter of only a few hundred nanometers. In the grinder, the 11-nm AuNPs mediated peak shift was three times smaller than the 150-nm AuNPs. In the anterior intestine, the peak shift was small with both AuNPs, which confirms that AuNPs can redisperse when the width of the intestinal lumen increases, returning to a lower degree of confinement. In this region, the presence of other biomolecules can result in the formation of a protein corona that may enhance the stability of the NPs [71–73], a notion which warrants further investigations but is not within the scope of this work. Remarkably, the aggregation of AuNPs is not irreversible, but associated with their temporary environment.

After 24 h of feeding, a significant amount of AuNPs accumulated in the posterior region of the gut, promoting low interparticle distance as the space narrowed, which resulted in a red-shift corresponding to ca. 5% of the initial peak position for both AuNPs. LM and TPLM studies showed that both NPs exhibited similar behavior in this region, which we believe is due to the mechanical pumping mechanism that governs the intestinal transit in *C. elegans* rather than being attributable to the AuNPs' properties.

The effect of the pH on NP status should also be considered (Fig. 5A). While the pH in the most anterior region of the gut is close to 6, it decreases to ca. 3.5 in the posterior part [45]. *In vitro* experiments showed that the combination of acidic pH and ionic strength of the citrate buffer pH 4.6 promoted the aggregation and precipitation of the AuNPs (Fig. S5). Therefore, these conditions may compromise AuNP stability in the most posterior part of the alimentary system.

In the rectal region, the presence of both AuNPs was sparse, which was likely due to the absence of food and thus reduced intestinal activity. However, when worms were transferred to a bacterial lawn and feeding commenced, the intestinal NPs were rapidly excreted in the form of micrometric ejections which were identical in color as the AuNPs observed inside the worm. The appearance of such ejections suggests that NPs were mixed with the intestinal content of the worm, typically food debris and endogenous secretions (Fig. 9), and suggests that the size of the AuNPs did not change. After 2 h of food consumption, AuNPs were no longer observed inside treated *C. elegans*.

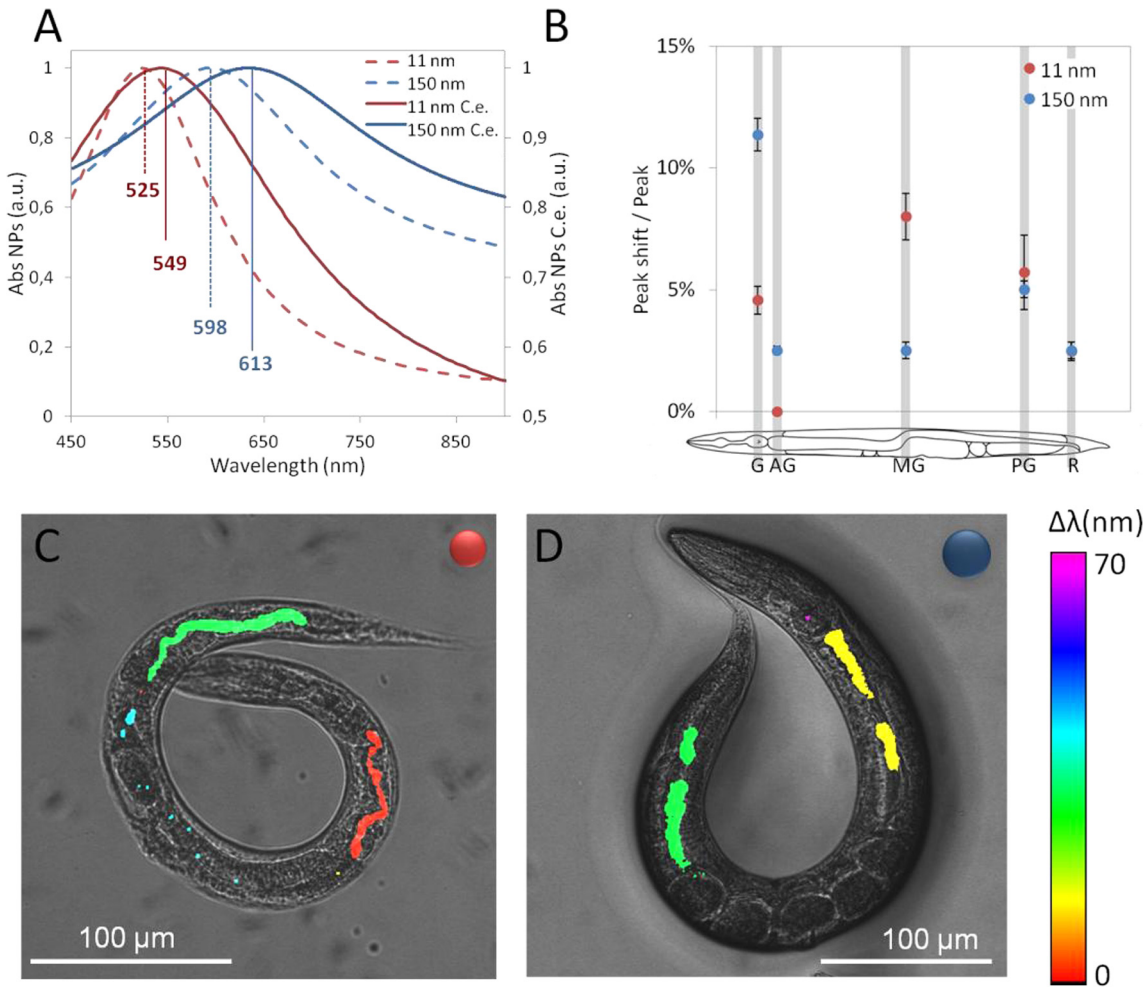

Fig. 8. A) Absorbance microspectroscopy of AuNPs as-synthesized (in water) and inside *C. elegans* expressed as the mean value of the different anatomical areas analyzed. B) Relative peak shift of the AuNPs in the different anatomical areas. (G: Grinder. AG: Anterior gut. MG: Mid-gut. PG: posterior gut. R: rectum). Error bars indicate standard deviation (SD) (n = 10). C–D) Absolute peak shift of the C) 11-nm and D) 150-nm AuNPs in the different anatomical areas (generated by merging LM and TPLM images).

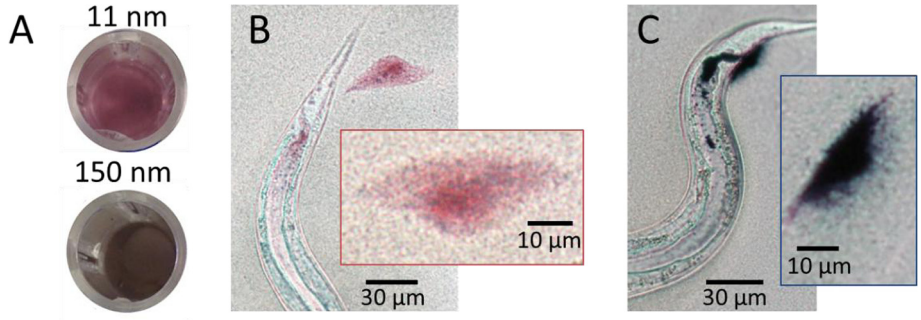

Fig. 9. Excretion of AuNPs onto the bacterial lawn when food is reintroduced. A) Colors of 11 and 150-nm AuNPs at 100 µg/mL (500 µL) in a 24-well plate. 11-nm AuNPs are pink and 150-nm brown in color. B–C) NP ejections after AuNPs-treated *C. elegans* are transferred to plates containing food. Excreted AuNPs maintain the color observed inside the worms. The appearance of the ejections suggests that NPs are mixed with organic contents inside the intestine of *C. elegans*. (For interpretation of the references to colour in this figure legend, the reader is referred to the web version of this article.)

4. Conclusions

By employing a combination of microscopy techniques (light microscopy, two-photon luminescence microscopy, and electron microscopy), chemical analysis, absorbance microspectroscopy and key life cycle endpoints, we were able to screen the biodistribution of 11-nm and 150-nm citrate-capped AuNPs in the model organism *Caenorhabditis elegans* at several levels, from the whole organism down to subcellular resolution. We confirm that the nanoparticles did not cross the intestinal and dermal barriers, based on the absence of endocytosis and adsorption, respectively, contradicting previous reports suggesting that similar-sized metal nanoparticles are endocytosed [60,61]. Moreover, our findings indicate that, *in vivo*, AuNP status is influenced by the physiological properties and the anatomical structure of this model organism, in particular modulating their degree of aggregation and changing

their optical properties inside the intestinal lumen where both acidic pH and the presence of biomolecules play an essential role. The transcription of selected markers of endocytosis and intestinal barrier integrity (*elt-2, eps-8, act-5, chc- 1 and dyn-1*) were not altered in worms exposed to AuNPs.

This study highlights how *C. elegans* can help to advance our understanding of meaningful nano/bio interactions at different biological levels, ranging from the whole animal down to cells and molecules. Here, we discern the effects of different AuNP sizes with potential applications as biocompatible nanomedicine products and safe cosmetics. This information is of particular relevance for the cosmetic, food, and pharmaceutical industries, as strict regulatory guidelines and high cost restrict the use of animals, especially during drug discovery and initial screening stages.

Acknowledgements

C. elegans N2 and *E. coli* OP50 were provided by the CGC, which is funded by NIH Office of Research Infrastructure Programs (P40 OD010440). This research was partially funded by the Spanish Ministry of Economy (MAT2015-64442-R, Ramon y Cajal program (AL, RyC-2010-06082), FPU program (LGM, FPU12/05549), Severo Ochoa Program (SEV-2015-0496) co-funded by European Social Funds), the Generalitat de Catalunya (2014SGR213), People Program of the European Commission (grant agreement no. 303630, co-funded by the European Social Fund), the Christian Boulin fellowship 2015 from EMBL (LGM), the COST Actions HINT (Action No. MP1202), and GENIE (Action No. BM1408-A). We acknowledge Víctor Fuentes for his collaboration in the synthesis of AuNPs. P. B., C. V. and R. Q. acknowledge the Spanish Ministry of Economy and Competitiveness, through the "Severo Ochoa" Programme for Centres of Excellence in R&D (SEV-2015-0522), Fundació Privada Cellex, and the CERCA Programme from the Generalitat de Catalunya. SRS acknowledges support by the RCUK (BBSRC – Biotechnology and Biological Sciences Research Council, grant BB/E025099/1).

Appendix A. Supplementary data

Supplementary data associated with this article can be found, in the online version, at http://dx.doi.org/10.1016/j.actbio.2017.01.080.

References

[1] M. Guix, C. Carbonell, J. Comenge, L. García-Fernández, A. Alarcón, E. Casals, Nanoparticles for cosmetics: how safe is safe?, Contrib Sci. (2010) 213–217.
[2] S. Kokura, O. Handa, T. Takagi, T. Ishikawa, Y. Naito, T. Yoshikawa, Silver nanoparticles as a safe preservative for use in cosmetics, Nanomed. Nanotechnol. Biol. Med. 6 (2010) 570–574.
[3] B. Gulson, M. McCall, M. Korsch, L. Gomez, P. Casey, Y. Oytam, A. Taylor, M. McCulloch, J. Trotter, L. Kinsley, G. Greenoak, Small amounts of zinc from zinc oxide particles in sunscreens applied outdoors are absorbed through human skin, Toxicol. Sci. 118 (2010) 140–149.
[4] X. Huang, M.A. El-Sayed, Gold nanoparticles: optical properties and implementations in cancer diagnosis and photothermal therapy, J. Adv. Res. 1 (2010) 13–28.
[5] P.K. Jain, K.S. Lee, I.H. El-Sayed, M.A. El-Sayed, Calculated absorption and scattering properties of gold nanoparticles of different size, shape, and composition: applications in biological imaging and biomedicine, J. Phys. Chem. B 110 (2006) 7238–7248.
[6] Organization for Economic Co-operation and Development OECD, List of manufactured nanomaterials and list of endpoints for phase one of the sponsorship programme for the testing of manufactured nanomaterials: Revision. Series on the Safety of Manufactured Nanomaterials No 272010.
[7] M. Bednarski, M. Dudek, J. Knutelska, L. Nowiński, J. Sapa, M. Zygmunt, G. Nowak, M. Luty-Błocho, M. Wojnicki, K. Fitzner, M. Tęsiorowski, The influence of the route of administration of gold nanoparticles on their tissue distribution and basic biochemical parameters: in vivo studies, Pharmacol. Rep. 67 (2015) 405–409.
[8] J.F. Hillyer, R.M. Albrecht, Gastrointestinal persorption and tissue distribution of differently sized colloidal gold nanoparticles, J. Pharm. Sci. 90 (2001) 1927–1936.
[9] A.N. Kharlamov, A.E. Tyurnina, V.S. Veselova, O.P. Kovtun, V.Y. Shur, J.L. Gabinsky, Silica-gold nanoparticles for atheroprotective management of plaques: results of the NANOM-FIM trial, Nanoscale 7 (2015) 8003–8015.
[10] M.E. Vance, T. Kuiken, E.P. Vejerano, S.P. McGinnis, M.F. Hochella, D. Rejeski, M. S. Hull, Nanotechnology in the real world: Redeveloping the nanomaterial consumer products inventory, Beilstein J. Nanotechnol. 6 (2015) 1769–1780.
[11] J. Suhag, H. Dureja, Cosmetic regulations: a comparative study, Skinmed 13 (2015) 191–194.
[12] L.P. O'Reilly, C.J. Luke, D.H. Perlmutter, G.A. Silverman, S.C.C. Pak, C. elegans in high-throughput drug discovery, Adv. Drug Deliv. Rev. 69–70 (2014) 247–253.
[13] P.M. Valencia, O.C. Farokhzad, R. Karnik, R. Langer, Microfluidic technologies for accelerating the clinical translation of nanoparticles, Nat. Nanotechnol. 7 (2012) 623–629.
[14] D.H. Hall, Z.F. Altun, C. Elegans Atlas, Cold Spring Harbor Laboratory Press, 2008.
[15] D.L. Riddle, T. Blumenthal, B.J. Meyer, J.R. Priess, C. elegans II, Cold Spring Harbor Laboratory Press, Cold Spring Harbor NY, 1997.
[16] L. Gonzalez-Moragas, A. Roig, A.C. Laromaine, Elegans as a tool for in vivo nanoparticle assessment, Adv. Colloid Interface Sci. 219 (2015) 10–26.
[17] A.D. Chisholm, T.I. Hsiao, The C. elegans epidermis as a model skin. I: development, patterning, and growth, WIREs Dev. Biol. 1 (2012) 861–878.
[18] A.D. Chisholm, S. Xu, The Caenorhabditis elegans epidermis as a model skin. II: differentiation and physiological roles, WIREs Dev. Biol. 1 (2012) 879–902.
[19] O. Bossinger, M. Hoffmann, Development and cell polarity of the C. elegans intestine, in: S. Najman (Ed.), Current Frontiers and Perspectives in Cell Biology, 2012.
[20] H.J.A. Egberts, J. Koninkx, J.E. Vandijk, J. Mouwen, Biological and pathobiological aspects of the glycocalyx of the small intestinal epithelium – a review, Vet. Q. 6 (1984) 186–199.
[21] J. Maury, C. Nicoletti, L. Guzzochambraud, S. Maroux, The filamentous brush-border glycocalyx, a mucin-like marker of enterocyte hyper-polarization, Eur. J. Biochem. 228 (1995) 323–331.
[22] G. Borgonie, M. Claeys, J. Vanfleteren, D. Dewaele, A. Coomans, Presence of peritrophic-like membranes in the intestine of 3 bacteriophagous nematodes (Nematoda, Rhabditida), Fundam. Appl. Nematol. 18 (1995) 227–233.
[23] M.J. Lehane, Peritrophic matrix structure and function, Annu. Rev. Entomol. 42 (1997) 525–550.
[24] K.M. Balla, E.R. Troemel, Caenorhabditis elegans as a model for intracellular pathogen infection, Cell. Microbiol. 15 (2013) 1313–1322.
[25] K. Sato, A. Norris, M. Sato, B.D.C. Grant, Elegans as a model for membrane traffic, WormBook: The Online Review of C elegans Biology (2014) 1–47.
[26] L. Wang, A. Audhya, In vivo imaging of C-elegans endocytosis, Methods 68 (2014) 518–528.
[27] Y. Zhao, Q. Wu, Y. Li, D. Wang, Translocation, transfer, and in vivo safety evaluation of engineered nanomaterials in the non-mammalian alternative toxicity assay model of nematode Caenorhabditis elegans, RSC Adv. 3 (2013) 5741–5757.
[28] J.S. Donner, S.A. Thompson, C. Alonso-Ortega, J. Morales, L.G. Rico, S.I.C.O. Santos, R. Quidant, Imaging of plasmonic heating in a living organism, ACS Nano 7 (2013) 8666–8672.
[29] I. Kolotuev, D.J. Bumbarger, M. Labouesse, Y. Schwab, Targeted ultramicrotomy: a valuable tool for correlated light and electron microscopy of small model organisms, Methods Cell Biol. 111 (2012) 203–222.
[30] J. Turkevich, P.C. Stevenson, J. Hillier, A study of the nucleation and growth processes in the synthesis of colloidal gold, Discuss. Faraday Soc. 11 (1951) 55–75.
[31] G. Frens, Controlled nucleation for the regulation of the particle size in monodisperse gold suspensions, Nat. Phys. Sci. 241 (1973) 20–22.
[32] C. Ziegler, A. Eychmüller, Seeded growth synthesis of uniform gold nanoparticles with diameters of 15–300 nm, J. Phys. Chem. C 115 (2011) 4502–4506.
[33] S. Brenner, The genetics of Caenorhabditis elegans, Genetics 77 (1974) 71–94.
[34] B. Sharma, A. Sharma, Future prospects of nanotechnology in development of anti-ageing formulations, Int. J. Pharm. Pharm. Sci. 4 (2012) 57–66.
[35] J.-h. Kim, C.-O. Hong, Y.-c. Koo, H.-D. Choi, K.-W. Lee, Anti-glycation effect of gold nanoparticles on collagen, Biol. Pharm. Bull. 35 (2012) 260–264.
[36] L. Gonzalez-Moragas, S.-M. Yu, E. Carenza, A. Laromaine, A. Roig, Protective effects of bovine serum albumin on superparamagnetic iron oxide nanoparticles evaluated in the nematode Caenorhabditis elegans, ACS Biomater. Sci. Eng. 1 (2015) 1129–1138.
[37] P. Pedrosa, R. Vinhas, A. Fernandes, P.V. Baptista, Gold nanotheranostics: proof-of-concept or clinical tool?, Nanomaterials 5 (2015) 1853–1879
[38] S.J. Soenen, W.J. Parak, J. Rejman, B. Manshian, (Intra)Cellular stability of inorganic nanoparticles: effects on cytotoxicity, particle functionality, and biomedical applications, Chem. Rev. 115 (2015) 2109–2135.
[39] S.W. Kim, S.H. Nam, Y.J. An, Interaction of silver nanoparticles with biological surfaces of Caenorhabditis elegans, Ecotoxicol. Environ. Saf. 77 (2012) 64–70.
[40] Q. Wu, Y. Li, M. Tang, D. Wang, Evaluation of environmental safety concentrations of DMSA Coated Fe2O3-NPs using different assay systems in nematode Caenorhabditis elegans, PLoS One 7 (2012) e43729.
[41] Q. Wu, W. Wang, Y. Li, Y. Li, B. Ye, M. Tang, D. Wang, Small sizes of TiO2-NPs exhibit adverse effects at predicted environmental relevant concentrations on nematodes in a modified chronic toxicity assay system, J. Hazard. Mater. 243 (2012) 161–168.

[42] S. Gupta, T. Kushwah, A. Vishwakarma, S. Yadav, Optimization of ZnO-NPs to investigate their safe application by assessing their effect on soil nematode Caenorhabditis elegans, Nanoscale Res. Lett. 10 (2015).
[43] A. Scharf, A. Piechulek, A. von Mikecz, Effect of nanoparticles on the biochemical and behavioral aging phenotype of the nematode Caenorhabditis elegans, ACS Nano 7 (2013) 10695–10703.
[44] A. Pluskota, E. Horzowski, O. Bossinger, A. von Mikecz, In Caenorhabditis elegans nanoparticle-bio-interactions become transparent: silica-nanoparticles induce reproductive senescence, PLoS One 4 (2009) e6622.
[45] V.M. Chauhan, G. Orsi, A. Brown, D.I. Pritchard, J.W. Aylott, Mapping the pharyngeal and intestinal pH of Caenorhabditis elegans and real-time luminal pH oscillations using extended dynamic range pH-sensitive nanosensors, ACS Nano 7 (2013) 5577–5587.
[46] M.R. Beversluis, A. Bouhelier, L. Novotny, Continuum generation from single gold nanostructures through near-field mediated intraband transitions, Phys. Rev. B 68 (2003).
[47] P. Ghenuche, S. Cherukulappurath, T.H. Taminiau, N.F. van Hulst, R. Quidant, Spectroscopic mode mapping of resonant plasmon nanoantennas, Phys. Rev. Lett. 101 (2008).
[48] J.P. Wilcoxon, J.E. Martin, F. Parsapour, B. Wiedenman, D.F. Kelley, Photoluminescence from nanosize gold clusters, J. Chem. Phys. 108 (1998) 9137–9143.
[49] M.B. Mohamed, V. Volkov, S. Link, M.A. El-Sayed, The 'lightning' gold nanorods: fluorescence enhancement of over a million compared to the gold metal, Chem. Phys. Lett. 317 (2000) 517–523.
[50] N. Gao, Y. Chen, L. Li, Z. Guan, T. Zhao, N. Zhou, P. Yuan, S.Q. Yao, Q.-H. Xu, Shape-dependent two-photon photoluminescence of single gold nanoparticles, J. Phys. Chem. C 118 (2014) 13904–13911.
[51] D. Yelin, D. Oron, S. Thiberge, E. Moses, Y. Silberberg, Multiphoton plasmon-resonance microscopy, Opt. Express 11 (2003) 1385–1391.
[52] H.F. Wang, T.B. Huff, D.A. Zweifel, W. He, P.S. Low, A. Wei, J.X. Cheng, In vitro and in vivo two-photon luminescence imaging of single gold nanorods, PNAS 102 (2005) 15752–15756.
[53] N.J. Durr, T. Larson, D.K. Smith, B.A. Korgel, K. Sokolov, A. Ben-Yakar, Two-photon luminescence imaging of cancer cells using molecularly targeted gold nanorods, Nano Lett. 7 (2007) 941–945.
[54] J. Park, A. Estrada, K. Sharp, K. Sang, J.A. Schwartz, D.K. Smith, C. Coleman, J.D. Payne, B.A. Korgel, A.K. Dunn, J.W. Tunnell, Two-photon-induced photoluminescence imaging of tumors using near-infrared excited gold nanoshells, Opt. Express 16 (2008) 1590–1599.
[55] J.D. McGhee, The Caenorhabditis elegans intestine, WIREs Dev. Biol. 2 (2013) 347–367.
[56] S.-M. Yu, L. Gonzalez-Moragas, M. Milla, A. Kolovou, R. Santarella-Mellwig, Y. Schwab, A. Laromaine, A. Roig, Bio-identity and fate of albumin-coated SPIONs evaluated in cells and by the C. elegans model, Acta Biomater. 43 (2016) 348–357.
[57] Q. Wu, L. Yin, X. Li, M. Tang, T. Zhang, D. Wang, Contributions of altered permeability of intestinal barrier and defecation behavior to toxicity formation from graphene oxide in nematode Caenorhabditis elegans, Nanoscale 5 (2013) 9934–9943.
[58] N. Mohan, C.-S. Chen, H.-H. Hsieh, Y.-C. Wu, H.-C. Chang, In vivo imaging and toxicity assessments of fluorescent nanodiamonds in Caenorhabditis elegans, Nano Lett. 10 (2010) 3692–3699.
[59] Q. Wu, Y. Li, Y. Li, Y. Zhao, L. Ge, H. Wang, D. Wang, Crucial role of the biological barrier at the primary targeted organs in controlling the translocation and toxicity of multi-walled carbon nanotubes in the nematode Caenorhabditis elegans, Nanoscale 5 (2013) 11166–11178.
[60] J.N. Meyer, C.A. Lord, X.Y. Yang, E.A. Turner, A.R. Badireddy, S.M. Marinakos, A. Chilkoti, M.R. Wiesner, M. Auffan, Intracellular uptake and associated toxicity of silver nanoparticles in Caenorhabditis elegans, Aquat. Toxicol. 100 (2010) 140–150.
[61] O.V. Tsyusko, J.M. Unrine, D. Spurgeon, E. Blalock, D. Starnes, M. Tseng, G. Joice, P.M. Bertsch, Toxicogenomic responses of the model organism Caenorhabditis elegans to gold nanoparticles, Environ. Sci. Technol. 46 (2012) 4115–4124.
[62] L. Kou, J. Sun, Y. Zhai, Z. He, The endocytosis and intracellular fate of nanomedicines: implication for rational design, Asian J. Pharm. Sci. 8 (2013) 1–10.
[63] E. Frohlich, E. Roblegg, Models for oral uptake of nanoparticles in consumer products, Toxicology 291 (2012) 10–17.
[64] J.D. McGhee, M.C. Sleumer, M. Bilenky, K. Wong, S.J. McKay, B. Goszczynski, H. Tian, N.D. Krich, J. Khattra, R.A. Holt, D.L. Baillie, Y. Kohara, M.A. Marra, S.J. Jones, D.G. Moerman, A.G. Robertson, The ELT-2 GATA-factor and the global regulation of transcription in the C. elegans intestine, Dev. Biol. 302 (2007) 627–645.
[65] J.D. McGhee, T. Fukushige, M.W. Krause, S.E. Minnema, B. Goszczynski, J. Gaudet, Y. Kohara, O. Bossinger, Y. Zhao, J. Khattra, M. Hirst, S.J. Jones, M.A. Marra, P. Ruzanov, A. Warner, R. Zapf, D.G. Moerman, J.M. Kalb, ELT-2 is the predominant transcription factor controlling differentiation and function of the C. elegans intestine, from embryo to adult, Dev. Biol. 327 (2009) 551–565.
[66] G.K. Hinkley, P. Carpinone, J.W. Munson, K.W. Powers, S.M. Roberts, Oral absorption of PEG-coated versus uncoated gold nanospheres: does agglomeration matter?, Part Fibre Toxicol. 12 (2015).
[67] C. Schleh, M. Semmler-Behnke, J. Lipka, A. Wenk, S. Hirn, M. Schaeffler, G. Schmid, U. Simon, W.G. Kreyling, Size and surface charge of gold nanoparticles determine absorption across intestinal barriers and accumulation in secondary target organs after oral administration, Nanotoxicology 6 (2012) 36–46.
[68] Y. Qu, W. Li, Y. Zhou, X. Liu, L. Zhang, L. Wang, Y.-f. Li, A. Iida, Z. Tang, Y. Zhao, Z. Chai, C. Chen, Full assessment of fate and physiological behavior of quantum dots utilizing Caenorhabditis elegans as a model organism, Nano Lett. 11 (2011) 3174–3183.
[69] C. Fang-Yen, L. Avery, A.D.T. Samuel, Two size-selective mechanisms specifically trap bacteria-sized food particles in Caenorhabditis elegans, PNAS 106 (2009) 20093–20096.
[70] K.H. Su, Q.H. Wei, X. Zhang, J.J. Mock, D.R. Smith, S. Schultz, Interparticle coupling effects on plasmon resonances of nanogold particles, Nano Lett. 3 (2003) 1087–1090.
[71] N. Feliu, D. Docter, M. Heine, P. Del Pino, S. Ashraf, J. Kolosnjaj-Tabi, P. Macchiarini, P. Nielsen, D. Alloyeau, F. Gazeau, R.H. Stauber, W.J. Parak, In vivo degeneration and the fate of inorganic nanoparticles, Chem. Soc. Rev. 45 (2016) 2440–2457.
[72] D. Docter, D. Westmeier, M. Markiewicz, S. Stolte, S.K. Knauer, R.H. Stauber, The nanoparticle biomolecule corona: lessons learned - challenge accepted?, Chem Soc. Rev. 44 (2015) 6094–6121.
[73] C.D. Walkey, J.B. Olsen, F. Song, R. Liu, H. Guo, D.W.H. Olsen, Y. Cohen, A. Emili, W.C.W. Chan, Protein corona fingerprinting predicts the cellular interaction of gold and silver nanoparticles, ACS Nano 8 (2014) 2439–2455.